Caspase-3 dependent peritubular capillary dysfunction is pivotal for transition from acute to chronic kidney disease after acute ischemia-reperfusion injury

Shanshan Lan[1,2,3], Bing Yang [1,2,3], Francis Migneault [1,2] Julie Turgeon [1,2], Maude Bourgault [1], Mélanie Dieudé [1,2,3], Héloïse Cardinal [1,2,3], Michael J. Hickey [5], Natacha Patey [1,3,4], Marie-Josée Hébert[* 1,2,3]

1. Research Centre, Centre hospitalier de l'Université de Montréal, Montreal, Quebec, Canada;
2. Canadian Donation Transplant Research Program, Edmonton, Alberta, Canada;
3. Université de Montréal, Montreal, Quebec, Canada;
4. Department of Pathology, Centre hospitalier universitaire Sainte-Justine, Université de Montréal, Montreal, Quebec, Canada;
5. Centre for Inflammatory Diseases, Monash University Department of Medicine, Monash Medical Centre, Clayton, Victoria 3168, Australia.

Running Head: Central role of PTCs in AKI to CKD transition

Corresponding author:

Dr. Marie-Josée Hébert

CRCHUM, Faculty of Medicine, Université de Montréal,

900, rue Saint-Denis, Montreal, Quebec, Canada, H2X 0A9

Phone: +1- 514 890-8000, poste 25017

Fax : +1- 514 412-7624

Email: marie-josee.hebert@umontreal.ca

Supplemental Material Available at :

https://doi.org/10.6084/m9.figshare.14782251
https://doi.org/10.6084/m9.figshare.13490847
https://doi.org/10.6084/m9.figshare.13490703

Abstract

Ischemia-reperfusion injury (IRI) is a major risk factor for chronic renal failure. Caspase-3, an effector responsible for apoptosis execution, is activated within peritubular capillary (PTC) in the early stage of IRI-induced acute kidney injury (AKI). Recently, we showed that caspase-3-dependent microvascular rarefaction plays a key role in fibrosis development after mild renal IRI. Here, we further characterize the role of caspase-3 in microvascular dysfunction and progressive renal failure in both mild and severe AKI, by performing unilateral renal artery clamping for 30/60 minutes with contralateral nephrectomy in wild-type (C57BL/6) or caspase-$3^{-/-}$ mice. In both forms of AKI, caspase-$3^{-/-}$ mice showed better long-term outcomes in spite of worse initial tubular injury. After 3 weeks, they showed reduced PTC injury, decreased PTC collagen deposition and α-SMA expression, and lower tubular injury scores when compared to wild-type animals. Caspase-$3^{-/-}$ mice with severe IRI also showed better preservation of long-term renal function. Intra-vital imaging and micro-computed tomography (microCT) revealed preserved PTC permeability and better terminal capillary density in caspase-$3^{-/-}$ mice. Collectively, these results demonstrate the pivotal importance of caspase-3 in regulating long-term renal function after IRI and establish the predominant role of PTC dysfunction as a major contributor to progressive renal dysfunction.

New and Noteworthy

Our findings demonstrate the pivotal importance of caspase-3 in regulating renal microvascular dysfunction, fibrogenesis, and long-term renal impairment after acute kidney injury (AKI) induced by ischemia-reperfusion injury (IRI). Furthermore, this study establishes the predominant role of peritubular capillary (PTC) integrity as a major contributor to progressive renal dysfunction post-IRI.

Introduction

Acute kidney injury (AKI) is one of the most powerful predictors of progressive renal failure in both native and transplanted kidneys (1). More than 20% of hospitalized adults worldwide experience some level of AKI (2-4) prompted most commonly by ischemia-reperfusion injury (IRI) and sepsis (5). IRI is an integral component of kidney transplantation and AKI occurs in 20%-50% of transplantations from deceased donors in the immediate postoperative period (6-8). The severity and number of AKI episodes in various patient cohorts predicts progressive long-term renal dysfunction and risk of end-stage renal failure (4, 9-12),. Long referred to as acute tubular necrosis, AKI is classically considered a disease of tubular epithelial cells. Increased cell death of tubular epithelial cells, in the form of apoptosis and necroptosis, is indeed an important characteristic of AKI and tends to occur predominantly at the cortico-medullary junction where blood and oxygen supply is limited (13). However, microvascular injury has emerged in the past decade as a major and previously underappreciated factor regulating progressive renal dysfunction after AKI (5, 14-16). Loss of peritubular capillary (PTC) favors chronic hypoxia leading to overexpression of hypoxia-inducible factor-1 α (HIF-1α) and fibrogenic factors which in turn favor myofibroblast differentiation and fibrosis (5, 15, 17-20). In transplanted kidneys, the magnitude of microvascular involution during the first 3 months following transplantation is a major negative predictor of long-term renal allograft function (21). Studies using in vivo imaging and electron microscopy demonstrated a tight correlation between PTC dysfunction/rarefaction and renal fibrosis in murine models of AKI and in human kidney biopsy samples (22-24).

Caspase-3 is an effector caspase responsible for the induction of apoptosis. Caspase-3 activation is present within PTC in the early stage of IRI-induced AKI (17, 25). Our group recently showed that caspase-3 dependent microvascular involution plays a predominant role in regulating the transition from AKI to fibrosis after mild renal IRI (26). Upon renal artery clamping, caspase-$3^{-/-}$ mice show early increases in tubular epithelial cell injury translating into more severe early renal dysfunction

than wild-type controls. Incapacity to mount an apoptotic response in caspase-3 deficient mice redirects tubular epithelial cell death towards necroptosis, a more severe and inflammatory type of cell death. Yet, in spite of increased early tubular cell death and acute renal dysfunction, PTC are largely protected from IRI-induced cell death. Inhibition of PTC apoptosis does not fuel other forms of regulated cell death but rather prevents microvascular rarefaction and long-term renal fibrosis. There is no impact of caspase-3 deficiency on long-term renal function. These results confirm a predominant role for microvascular injury over early epithelial injury as a driver of renal fibrosis after IRI.

Renal fibrosis is classically considered a surrogate marker of progressive renal failure. Yet, recent data suggest that progressive renal dysfunction after AKI is not always correlated with renal fibrosis (24). Having identified a predominant role for caspase-3-dependent microvascular injury in renal fibrogenesis after mild IRI, we now aim at evaluating the impact of caspase-3 on microvascular function and integrity, fibrogenesis and renal function after severe IRI. In the present study, we compare early and late microvascular and tubular abnormalities in caspase-3 deficient mice exposed to mild and severe forms of IRI. Our goal is to assess whether caspase-3 deficiency preserves microvascular integrity and function even in severe forms of AKI or rather increases PTC injury, as was the case for renal epithelial cells in mild forms of AKI.

Materials and Methods

Animal and Surgical Procedures

We used 6-8 weeks old female C57BL/6 mice from Charles River Laboratories (Wilmington, MA,USA). CASP3-deficient (caspase-$3^{-/-}$) mice on a C57BL/6 congenic background, aged 6–8 weeks, were derived from breeding pairs of heterozygous CASP3-deficient (B6.129S1-C3tm1Flv/J) mice obtained from Jackson Laboratory (stock #006233; Bar Harbor, ME). The generation of these mice was previously described (26). These homozygote mice were viable, reached adulthood, and

showed a variety of hyperplasias and disorganized cell deployment in the brain. All mice were kept in 12-hour light/dark cycles, with normal food provided ad libitum. IRI by unilateral renal artery clamping plus contralateral nephrectomy was performed as described previously (26). Detailed surgical procedures can be found in Supplemental Material. Animals were divided into mild AKI (IR30m) and severe AKI (IR60m) and were sub-grouped into pre-operation, SHAM, 1 day, 2 days, 7 days, and 21 days post-operation groups. A maximum of 10 mice per sub-group were used. The number of mice per experiment is described in figure legends. Carprofen was injected subcutaneously daily until day 3 post-op. Mice with significant body weight loss were also injected with 0.5 mL saline + 0.3 mL 2,5% dextrose. Mice were euthanized by neck dislocation, after performing cardiac puncture under 2% isoflurane inhalation at baseline or on days 1, 2, 7, or 21 post-surgery and the left kidney, serum, and urine were collected.

Renal Function Biochemical Evaluation

Serum creatinine levels were determined using Vitro CREA slides and Vitro chemistry products (Vitro 250/350 Chemistry System; Ortho Clinical Diagnostics, Raritan, NJ), as described in our previous work (26, 27).

Renal Histopathological Examination

Tubular Injury Score

Tubular injury score was evaluated in murine renal tissue stained with haematoxylin and eosin (HE), as described previously (26). Ten high-power magnification fields (200X) were randomly chosen; five from the renal cortex and five from the cortico-medullary junction. Based on the percentage of affected tubules, the tubular injury score was classified as 0-5 (0: normal; 1: mild injury, involvement of 0%–10%; 2: moderate injury, involvement of 11%–25%; 3: severe injury, involvement of 26%–49%; 4: high severe injury, involvement of 50%–75%; 5: extensive injury, involvement of 75%). The criteria for tubular injury involved: brush border loss, tubular dilation, cast formation, tubular necrosis,

as well as neutrophil infiltration. All assessments were done by two investigators blinded to experimental conditions (28).

Peritubular Capillary Vascular Congestion

Rouleaux formation, a read-out of peritubular capillary microvascular congestion, was estimated by counting accumulated erythrocytes inside peritubular capillaries (PTC) on HE-stained slides. Ten randomly chosen high magnification fields were counted per mouse by two investigators blinded to experimental conditions.

Immunohistochemistry

Mice were sacrificed at different time points (baseline, days 1, 2, 7 and 21). Kidneys were collected and fixed in 10% formalin, embedded in paraffin, and subsequently cut into 4-µm slices. Immunohistochemistry staining was performed on paraffin-embedded tissue as described previously (26). The antibodies used in this study were mouse endothelial cell antigen (MECA-32; 1:20; 120501; Biolegend, San Diego, CA, USA), HIF-1α (1:200; ab2185; Abcam,Cambridge, MA, USA), α-smooth muscle actin (α-SMA; 1:200, clone 1A4; Dako, Santa Clara, CA,USA). Stained slides were scanned (original magnification 200X) using an Olympus VS110 slide scanner and randomly chosen fields were evaluated. Quantification of MECA-32 staining in PTC were assessed by evaluating the ratio of positive PTC/ tubule number in five high-power magnification fields (200X) in cortical-medullary junction, and MECA-32 in glomeruli was quantified by accounting positive glomerulus in cortex in five high-power magnification fields (100X). Quantification of α-SMA staining in PTC were assessed by accounting positive PTC in ten high-power magnification fields (200X); α-SMA staining in glomeruli was performed in five high-power magnification fields (100X). All assessments were done by two independent investigators blinded to experimental conditions. α-SMA staining in renal microvessels was assessed using Visiomorph TM VIS Histoinformatics Software (Olympus) in the whole kidney.

Sirius Red Staining

Sirius Red staining was performed using Picro-Sirius Red Staining Kit (ab150681, Abcam, Cambridge, MA, USA) according to the manufacturer's instructions. All slides were scanned using an Olympus VS110 slide scanner microscope. Five randomly chosen high-power fields at the cortical-medullary junction (magnification 200X) were taken. Sirius red positive area within PTC and glomeruli were evaluated with ImageJ (National Institutes of Health) by two independent investigators blinded to experimental conditions.

Silver staining

Silver staining was done according to Jones' Methenamine Silver Stain (JMS) - Staining protocol (29). Stained slides were scanned using an Olympus VS110 slide scanner microscope. Five randomly chosen high-power fields in the renal cortical section (magnification 200X) were taken, and glomerulosclerosis scores were evaluated by two independent investigators blinded to experimental conditions. Based on involved glomerular percentage, glomerulosclerosis score was classified as 0-3 (0: no glomerulopathy-double contours affecting <10% peripheral capillary loop in the most severe attacked glomerulus. 1: double contours affecting up to 25% peripheral capillary loop in most affected non-sclerotic glomeruli. 2: double contours affecting up to 50% peripheral capillary loop in most affected non-sclerotic glomeruli. 3: double contours affecting >50% peripheral capillary loop in most affected non-sclerotic glomeruli) (30).

Electron Microscopy

Fresh murine renal tissue was fixed with 3% glutaraldehyde, post-fixed with 1% osmium tetroxide and embedded in Epon according to routine techniques. Ultrathin renal slices were obtained using an ultra-microtome (Leica Biosystems RM2245, Buffalo Grove, IL, USA) and mounted on naked nickel grids. Slices were stained with aqueous uranyl acetate and lead citrate as previously reported (31). Examination was performed using a Zeiss Axio Imager.A1 transmission electron microscope and electron micrographs were captured using a AxioCam, Zeiss digital camera. Images of renal

peritubular capillaries were taken randomly in the cortex and cortico-medullary junction by two blinded investigators.

Ex-vivo renal microvasculacular microCT imaging

5 mL silicone rubber radiopaque contrast agent Microfil (Flow Tech Inc. Carver, MA, USA) was pump-perfused (0.5ml/min, catheter length: 12cm) via a left ventricle 23G catheter to allow 3D visualization of the renal microvasculature. The kidney was collected following polymerization for 4-6 hours at 4 °C and fixed in 1.5 mL tube for subsequent scan procedure (32, 33).

Ex-vivo micro-Computed Tomography (microCT) manipulation was performed using a high-resolution SkyScan 1176 scanner (SkyScan, Kontich, Belgium). The fixed kidney was positioned and scanned 360° around the vertical axis with a rotating speed of 0.3°, at a resolution of 9 um. Vascular volume was assessed following volume rendering and 3D reconstruction analysis (22). Terminal capillaries were counted using Imaris 9.2 software (Oxford Instruments plc).

Assessment of vascular permeability

Evans Blue (E2129, Sigma Aldrich, Burlington, MA, USA) (5mg/kg) was dissolved in D-PBS 1X (1 g/L glucose, 36 mg/L sodium pyruvate with calcium and magnesium) and injected intravenously via the tail vein. After 30 min of circulation, mice were perfused with 20 mL of 0,9% NaCl via the left ventricle to remove all the blood in the circulation. The ischemic kidney was collected, dried, weighed, and put in 100% formamide (4ml/g) at 56°C for 24h. Extracted Evans Blue was measured by spectrophotometry at 620 nm and expressed as mg/g bodyweight (34, 35).

Intra-vital mice kidney imaging

Intra-vital images were acquired using an upright Olympus FV1000 laser scanning confocal microscope (Olympus, Japan). At 21 days post-ischemia-reperfusion, mice were anesthetized with 2% isoflurane and 1% oxygen over all the surgery procedure and imaging session. Then mice were

placed on a 37°C heated blanket with the right jugular vein catheterized for the administration of reagents. The kidney was exposed by dorsal incision and positioned on a special stage (36). After preparation procedure, mice were maintained under a 32°C environment and were monitored using Mouse Ox apparatus (Flow Tech Inc). All images were acquired using a XLUM Plan FL N 20x/1.00 Water objective. Ultrasound gel was used to establish the immersion between the objective and the coverslip (#1.5, 0.17 mm) as it has the same refractive index as water. 2000 kDa Alexa Fluor 488 (AF488)-conjugated dextran (FD 2000S, Sigma Aldrich, Burlington, MA, USA) (0.25 mg/kg) and Evans Blue (1 mg/kg) were injected via a jugular catheter. Live imaging was taken at pre-injection and 15 minutes post-injection. For excitation, 405 nm, 488 nm and 635 nm lasers were used simultaneously for detection of autofluorescence (AF), Dextran AF488 and Evans Blue, respectively. For detection, photomultiplier tubes (PMT) detectors were configured as follows: for AF detection, a SDM490 dichroic mirror was positioned in front of the first PMT associated with a 430-470 nm emission filter; for Dextran AF488 detection, a SDM560 dichroic mirror was positioned in front of the second PMT, associated with a 505-605 nm emission filter; and for Evans Blue detection, a 655-755 nm emission filter was positioned in front of the third detector. All channels were acquired simultaneously. Images were acquired in a 640x640 pixel format at zoom 3 (pixel resolution of 331 nm) at 4 µs/pixel speed at different time points after Evans Blue injection: prior to injection, 30 sec, 3 min, 5 min, 10 min and15 min post-injection. For live videos, the frame interval between each image was 2.4 seconds. During live acquisition, the sample was scanned in x and y at zoom 1X until a region of interest was observed during or after Evans Blue injection. The zoom was then adapted to Zoom 3X to focus on this specific region of the kidney. For some interesting time-points/localizations, z-stacks were acquired as followed: zoom 3X, step size 2 µm, Z volume between 22 µm up to 44 µm depth. Images were acquired using the Olympus Fluoview software (v4.2.3.6, Olympus, Japan). Final images are 12 bits. Image analysis was performed using FIJI software (NIH, open source).

Quantification of microvascular permeability was assessed by measuring the number of sites of Evans Blue accumulation per field of view. Capillary perfusion was evaluated by quantification of perfused versus non-perfused capillaries in each field. A capillary branch was defined as one segment between two nearby endpoints. Perfused capillaries with circulation were defined as yellow/green fluorescence in the lumen, and visible red blood cell circulation; non-perfused capillaries were defined as weak red fluorescence and the absence of cell circulation (34). Perfused capillaries without circulation were defined as yellow/green fluorescence in the lumen but without cellular circulation.

Statistics

All data were expressed as means ± SEM. Biological and histological data were compared using unpaired *t*-test. Statistical analyses were performed using Prism 8 (Prism-GraphPad software, Inc). P values of 0.05 or less were considered significant.

Study approval

All animal experimental protocols (document number for animal use approval: 4I14057MJHs and IP18047MJHs) were reviewed and approved by the Centre hospitalier de l'Université de Montréal - Comité Institutionnel de Protection des Animaux.

Results

Caspase-3 deficiency preserves long-term renal function after severe AKI.

We showed previously that caspase-3 deficiency prevents microvascular rarefaction and long-term renal fibrosis after mild renal IRI despite early accentuation of tubular injury (26). We now compare the impact of caspase-3 deficiency in severe vs mild forms of IRI-induced AKI. Severe AKI was induced by clamping the renal artery for 60 minutes and mild AKI with renal artery clamping for 30 minutes. Both interventions were followed by contralateral nephrectomy. Serum creatinine levels were significantly higher in severe AKI compared to mild AKI, both in wild-type and caspase-$3^{-/-}$ mice

at all time points (Fig. 1A). In caspase-3$^{-/-}$ mice, creatinine levels were significantly higher at day 1 and 2 post-IRI in mild AKI compared with wild-type controls (Fig. 1B). In the severe AKI groups, there was no difference in serum creatinine levels between caspase-3$^{-/-}$ mice and wild-type controls during the first-week post-IRI. At day 21 post-IRI, serum creatinine failed to go back to baseline in both wild-type and caspase-3$^{-/-}$ mice with severe AKI (Fig. 1A). Serum creatinine levels were statistically lower in caspase-3$^{-/-}$ mice with severe AKI compared with wild-type controls with severe AKI but there was no significant difference in mild AKI. Caspase-3$^{-/-}$ mice showed higher tubular injury scores than wild-type controls in both mild and severe AKI at day 1 post-IRI. These results are in line with our previous findings showing redirection towards tubular necroptosis in caspase-3$^{-/-}$ mice in the early phase of AKI (26). On day 21 post-IRI, tubular injury scores were significantly better in caspase3$^{-/-}$ mice compared to wild-type controls in both severe and mild AKI (Fig. 1B). Collectively, these results demonstrate that the severity of IRI predicts long-term renal dysfunction while early tubular injury does not predict long-term tubular integrity and level of renal dysfunction (Fig. 1B, Fig. S1A).

Caspase-3 deficiency improves long-term renal microvascular integrity and rarefaction after mild and severe forms of IRI-induced AKI.

Microvascular rarefaction is increasingly recognized as an important determinant of progressive renal failure after AKI (24, 37, 38). Therefore, we turned to evaluating the impact of caspase-3 on microvascular integrity in mild and severe forms of AKI (37). Rouleaux formation, a read-out of microvascular congestion, increased in the early phase of AKI in wild-type mice submitted to 30 min of artery clamping and increased further on the long term, suggesting sustained and progressive abnormalities in microvascular circulation (Fig. 1C). Caspase-3$^{-/-}$ mice showed significantly lower rouleaux levels both in the early (day 1) and chronic (day 21) phases of mild AKI (Fig. 1C, Fig. S1B). Intriguingly, severe AKI was associated with lower levels of rouleaux formation in wild-type and caspase-3$^{-/-}$ mice compared to mild AKI. Rouleaux formation at day 21 was significantly lower in

caspase-3$^{-/-}$ mice with severe AKI compared with wild-type mice. These results suggest better preservation of microvascular circulation in caspase-3$^{-/-}$ mice, both in mild and severe forms of AKI. The lower levels of rouleaux formation with severe AKI were surprising and raised the possibility of enhanced microvascular rarefaction with severe AKI, preventing microvascular circulation and hence rouleaux formation. To test this possibility, we used immunostaining of murine endothelial cell antigen-32 (MECA-32), a marker of microvascular endothelial cells (34). On day 21 post-IRI, MECA-32 staining in cortico-medullary PTC was significantly reduced in wild-type mice exposed to mild AKI compared to sham-treated animals. MECA-32 was further reduced in wild-type mice exposed to severe AKI compared to sham. In both forms of AKI, caspase-3$^{-/-}$ mice showed significantly higher PTC MECA-32 staining than wild-type counterparts. (Fig. 2A, Fig. S2). Electron microscopy also revealed the preservation of microvascular integrity in caspase-3$^{-/-}$ mice. Features of endothelial apoptosis, such as nuclear condensation, apoptotic bodies, apoptotic exosome-like vesicles, were found within PTC in wild-type but not in the caspase-3$^{-/-}$ mice (Fig. 3A-F). Rouleaux formation was also observed in PTC of wild-type mice, consistent with results on HE-stained tissue (Fig.1C). Wild-type mice also showed reduced endothelial fenestration and basement membrane irregularities at 21 d post-IRI (Fig. 3A-C). These features were limited in caspase-3$^{-/-}$ mice, where microvascular integrity was better preserved. (Fig. 3D-F). Caspase-3 immunohistochemistry staining revealed the presence of several positive endothelial-like cells within PTC in wild-type mice at 21 days post severe IRI (Fig. S3) unlike caspase-3$^{-/-}$ mice. Collectively, these results showed enhanced microvascular rarefaction with more severe forms of AKI and better PTC preservation in caspase-3 deficient mice. We also evaluated whether microvascular compartments other than PTC show differences in MECA-32 staining post-AKI. Glomerular MECA-32 staining was not modulated by AKI in wild-type or caspase-3$^{-/-}$ mice (Fig. 2B). In line with this result, glomerulosclerosis was not modulated post-AKI (Fig. S4). To further confirm these results, we assessed microvascular rarefaction with contrast-enhanced microCT. Total blood vessel volume decreased at day 21 post-IRI in mild and severe AKI when compared to baseline. There was however no significant difference between wild type and caspase-3$^{-/-}$ mice (Fig. 4). However, significant differences were noted when

considering terminal capillary volume. In wild-type mice, the number of terminal capillaries was lower than baseline in mild AKI and there was a further significant reduction in severe AKI. Caspase-3$^{-/-}$ mice showed significantly higher terminal capillary numbers than wild-type counterparts after mild and severe AKI (Fig. 4C). Collectively, these results demonstrate the importance of caspase-3 in controlling microvascular rarefaction in both mild and severe forms of AKI.

Caspase-3 deficiency prevents endothelial permeability disorder after mild and severe AKI. Abnormal microvascular permeability is another feature of AKI to CKD transition and is thought to contribute to the development of a hypoxic microenvironment that fuels fibrogenesis, tubular injury and renal failure (37). We evaluated endothelial permeability post-IRI using intra-vital confocal microscopy. Mice were injected with fluorescein isothiocyanate–labeled high molecular weight (2000 kDa) dextran to delineate the vasculature and with red fluorescent Evans Blue to detect extravasation. Evans Blue binds to albumin, which make it capable of labeling the endothelial sites of albumin leakage. At day 21 post-IRI, wild-type mice with mild AKI showed abnormal PTC permeability with significantly increased global kidney Evans Blue extravasation compared with sham-treated mice (Fig. 5D). Caspase-3$^{-/-}$ mice with mild AKI showed reduced Evans Blue extravasation when compared to wild-type controls. There was however no difference between wild-type and caspase-3$^{-/-}$ mice with severe AKI. We went on to characterize microscopic differences. Wild-type mice exposed to mild AKI showed areas of extravasation, the number of which was further enhanced in wild-type mice exposed to severe AKI. These extravasation areas were characterized by the presence of extravascular Evans Blue but not 2000 kDa dextran. We observed the appearance of Evans Blue within the peritubular or tubular lumen shortly after I.V. administration suggesting respectively PTC and glomerular filtration barrier dysfunction after IRI (video 5-8). By performing intra-vital imaging, we could also assess microvascular perfusion in real time. In both mild and severe AKI, caspase-3$^{-/-}$ mice showed significantly reduced length of non-perfused PTC when compared to wild-type mice (Fig. 5A, B, Video 1, 2, Fig. S5). The ratio of perfused capillaries decreased in wild-type mice exposed to mild AKI when compared to baseline and the decrease was

further enhanced in wild-type mice exposed to severe AKI (Fig. 5C). Caspase-3$^{-/-}$ kidneys showed a higher number of perfused capillaries in mild and severe AKI as compared to wild-type kidneys (Fig. 5C, Video 3, Video 4, Fig. S6, Video 9). Prevention of PTC rarefaction leading to preservation of tubule perfusion was also reflected by lower expression of tubular HIF-1a in caspase-3$^{-/-}$ mice at 21 days post-IRI both in the cortex and cortico-medullary junction (Fig. S7). Collectively, these results demonstrate that AKI of increasing severity leads to enhanced permeability disturbances and that caspase-3 controls microvascular integrity and permeability after mild and severe AKI.

Caspase-3 deficiency prevents renal fibrogenesis after AKI.

Progressive renal failure is classically accompanied by fibrosis characterized by increased collagen deposition and interstitial myofibroblast differentiation. Renal microvascular disturbances are frequently associated with renal fibrogenesis although recent data suggest that this association may not always hold true (24). Staining with Sirius red, a marker of collagen I and III, revealed a significant increase in peritubular collagen deposition at day 21 post-IRI in wild-type mice exposed to mild and severe AKI. Caspase-3 deficient mice showed reduced collagen deposition as compared with wild-type controls in both mild and severe forms of AKI (Fig. 6A). Increased collagen deposition with AKI was not present in all microvascular compartments as Sirius red staining in glomeruli was not modulated by AKI in wild-type or caspase-3$^{-/-}$ mice at day 21 post-IRI (Fig. 6B). Electron microscopy confirmed the accumulation of collagen within the peritubular basement membrane in wild-type mice (Fig. 6C).

Myofibroblast differentiation, as evaluated with alpha-smooth muscle actin (α-SMA) staining, was assessed in PTC and glomeruli. On day 21 post-IRI, wild-type mice showed increased peritubular α-SMA staining in both forms of AKI. In both mild and severe forms of AKI, caspase-3$^{-/-}$ mice demonstrated less myofibroblast differentiation within renal PTC (Fig. 7A, B). However, there was no difference in α-SMA staining within glomeruli or macrovessels between wild-type or caspase-3 deficient mice (Fig. 7C, D). Collectively, these results highlight the association between PTC

abnormalities and fibrogenesis and confirm the protective role of caspase-3 deficiency in preventing peritubular fibrosis.

Discussion

Microvascular rarefaction is increasingly appreciated as an important predictor of AKI to CKD transition following ischemia-reperfusion injury. Here we show that caspase-3 is a pivotal regulator of peritubular microvascular integrity and long-term dysfunction after IRI. The severity of acute IRI correlates in the long term with the severity of microvascular rarefaction, fibrosis, and loss of renal function. Severe AKI also leads to greater long-term perturbation of renal microvascular permeability (Fig. 8). We identify caspase-3 as a pivotal factor controlling microvascular homeostasis and renal function post-IRI. These results extend our previous observations pointing to an important role for caspase-3 in the regulation of microvascular rarefaction following mild IRI. In this study, we show that in mild and severe forms of AKI, caspase-3 control not only the number of surviving peritubular capillaries but also impacts their permeability and overall tubule-interstitial oxygenation. The beneficial impact of caspase-3 deficiency on long-term renal outcomes is present despite the early deterioration of epithelial injury, both in mild and severe forms of AKI, confirming the predominant role of microvascular injury over early epithelial damage in regulating AKI to CKD transition.

A number of different murine IRI models (39-42) are available to investigate the pathophysiology of AKI-to-CKD transition. However, severe forms of AKI are less commonly investigated given the difficulty of ensuring animal survival in the long term (43, 44). Head-to-head comparisons of microvascular abnormalities after mild and severe IRI are therefore still lacking. Yet severe AKI is an important cause of progressive renal dysfunction in patients (45) and efforts are needed to better understand the mechanisms contributing to progressive renal failure in this context. In this study, we used unilateral renal artery clamping for 30 and 60 minutes along with contralateral nephrectomy, as means of comparing mild and severe forms of IRI on AKI-to-CKD transition. As expected, severe AKI led to higher serum creatinine levels at all time points when compared to mild AKI. Intriguingly,

indices of microvascular congestion 2 days and 3 weeks after IRI were significantly less important in severe AKI compared to mild AKI. This finding led us to consider the possibility that severe IRI aggravates microvascular drop-out. In that case, congestion indices would be reduced not because of better microvascular integrity but rather by the disappearance of the microvascular network. Our results largely support this assumption. Immunohistochemistry for MECA-32, electron microscopy and *in vivo* imaging with 3D integral renal vasculature visualization confirmed enhanced and accelerated microvascular rarefaction with increased severity of IRI. Caspase-3 deficiency led to better preservation of the renal peritubular microvasculature both in mild and severe forms of AKI. 3D reconstructed kidney from microCT imaging showed enhanced reduction of terminal capillary volume with increasing severity of IRI and preservation of capillary volume in caspase-3 deficient animals. Microvascular analysis along with endothelial staining confirmed PTC rarefaction but showed no difference in glomerular histology in both forms of AKI. These findings are in line with observations showing little ultrastructural alterations of glomerular endothelial membranes following renal ischemia-reperfusion injury (46, 47).

Our results also point to caspase-3 as a pivotal regulator of PTC injury and dysfunction. IRI triggers breaks of intercellular adhesions leading to increased PTC permeability exemplified by leakiness of the contrast agent (48). Enhanced permeability likely represents a compensation mechanism aimed at preserving tissue perfusion after ischemia. However, in the long-term, leakiness leads to interstitial edema, capillary compression, and further perturbations in perfusion and oxygenation (49). Using intra-vital kidney imaging, we found abnormal PTC leakiness with mild IRI and further enhanced permeability abnormalities with severe IRI. Enhanced capillary rarefaction with severe IRI was associated with more severe permeability disturbances and higher tubular expression of HIF-1α. Conversely, caspase-3 deficiency protected against permeability disturbances and microvascular drop-out and was associated with lower HIF-1α tubular levels. These results are in line with previous findings suggesting a major role for microvascular injury in fueling tubular ischemia that can, in turn, contribute to CKD transition (50). Microvascular permeability disturbances similar to the ones we

419 described after severe IRI injury have been reported in association with a number of animal models
420 of renal dysfunction such as ureteral obstruction and Col4a3-deficient mice, and in patient biopsy
421 samples with progressive renal failure due to glomerulonephritis and interstitial nephritis (34). These
422 similarities raise the possibility that microvascular rarefaction and permeability disturbances
423 represent a common pathway of transition toward progressive loss of renal function, irrespective of
424 the initial cause of renal dysfunction.
425 Renal fibrosis is a classical hallmark of progressive renal failure. The present work highlights a close
426 association between the severity of microvascular disturbances, level of peritubular fibrosis, and loss
427 of renal function. There was however no correlation between indices of early tubular injury and long-
428 term renal fibrosis or renal function. In caspase-3 deficient mice, early renal dysfunction and tubular
429 injury scores were worse than wild-type controls in both forms of IRI. Yet caspase-3 deficient mice
430 showed lower renal fibrosis and reduced dysfunction in the long term. Collectively, our results point
431 to the importance of turning our attention to markers of microvascular injury as potential predictors of
432 AKI to CKD transition. Currently, AKI severity is evaluated with clinical criteria, such as an increase
433 in serum creatinine, decreased urine output, and the need for renal replacement therapy. Most
434 biomarkers of AKI, such as cystatin C, kidney-injury-molecule-1 (KIM-1), and neutrophil gelatinase-
435 associated lipocalin (NGAL) monitor levels of tubular injury (51, 52). However, the present results
436 and an increasing body of literature suggest that early tubular injury is unlikely to predict transition to
437 CKD if not associated with concomitant microvascular injury and PTC drop-out (53, 54). There is an
438 urgent need for biomarkers that could allow a reliable and non-invasive assessment of the degree of
439 PTC damage following IRI. Several new candidates are emerging and should be the scope of future
440 studies. Our group showed that endothelial cells release apoptotic exosome-like membrane vesicles
441 which can be tracked in circulation following ischemia-reperfusion episodes, including renal IRI (55).
442 Several endothelial associated proteins and molecules have been considered as potential biomarker
443 candidates at an early stage, such as E-selectin, P-selectin, vascular endothelial growth factor
444 (VEGF), glycocalyx, endothelin-1, angiopoietins, intercellular adhesion molecule (ICAM), vascular

cell adhesion molecule (VCAM) (56-62). It will be crucial to assess the capacity of these biomarkers and others to predict AKI to CKD transition and long-term renal outcomes after IRI. As acute microvascular dysfunction following IRI has been documented in lungs, liver and intestine (63-66), better means of assessing microvascular damage could prove useful in delineating the relationship between microvascular drop-out and fibrosis in a number of conditions.

Our results also point to caspase-3 as a potential target of intervention for the prevention of CKD transition following AKI. Caspase-3 inhibitors and siRNA have been tested on early renal outcomes in a number of IRI animal models with somewhat conflicting results (67-70). Caspase-3 siRNA intervention also displayed a protective role on renal function in a porcine kidney autotransplant model (70). Although caspase inhibition has yet to be tested in human renal IRI, a pan-caspase inhibitor has been evaluated in clinical trials in the context of liver transplantation (NCT00080236), IDNN-6556 (pan-caspase inhibitor) administration in cold perfusate protected liver damage against IRI initiated apoptosis (71). But, to our knowledge, only early time points were assessed. Further clinical studies addressing the use of caspase inhibition in the prevention of progressive renal dysfunction after IRI are still lacking. Our current results point to the need to address this question in future clinical studies that will look into acute and long-term consequences of renal IRI in patients.

In conclusion, the severity of PTC disturbances after IRI is a major predictor of AKI to CKD transition. Caspase-3 is an important mediator in AKI, due to its crucial regulatory effect on apoptosis and its downstream consequence on microvascular function and rarefaction, fibrogenesis, and renal function post-IRI. These results open new directions for defining predictors of AKI to CKD transition and identify caspase-3 as a novel target of intervention for preserving long-term renal function.

Author contributions

S.L. and MJ.H. conceived and designed the research strategy. S.L. and B.Y. performed experiments. S.L., B.Y., M.J.H., MJ.H., and N.P. analyzed the slides, images and videos. S.L., B.Y., F.M., J.T., M.B., M.D. analyzed data. S.L., B.Y., F.M., J.T., M.D., M.J.H., H.C., and MJ.H. interpreted the results.

S.L. and F.M. prepared figures. S.L., F.M., and MJ.H. drafted the manuscript. S.L., F.M., H.C., and MJ.H. edited and revised the manuscript. S.L., B.Y., F.M., J.T., M.B., M.D., M.J.H., H.C., N.P., and MJ.H. approved the final version of the manuscript.

Acknowledgment

The authors acknowledge support from the Canadian Institutes of Health Research (MOP-123436 and PJT-148884) and the Canadian Donation Transplantation Research Program (CDTRP). Marie-Josée Hébert holds the Shire Chair in Nephrology, Transplantation and Renal Regeneration of Université de Montréal. We also thank the J.-L. Lévesque Foundation for renewed support. Shanshan Lan was supported by the Canadian Society of Transplantation (CST) Research Training Award and is a CDTRP trainee. We thank Dr. Junzheng Peng of the Cardiovascular phenotype core facility of the Centre Hospitalier de l'Université de Montréal Research Centre (CRCHUM) for assisting in microCT imaging and Dr. Aurélie Cleret-Buhot of the Cell Imaging core facility of the CRCHUM for performing the confocal microscopy acquisitions. We thank the CRCHUM molecular pathology platform and animal facility for their service. Many thanks to Dr. Shijie Qi for thoughtful advice and to Hyunyun Kim for his assistance with murine renal pathology evaluation. Also great thanks to Dr. Kejia Zhang for his drawing contribution in Figure 8 and graphic abstract.

The authors have no conflict of interest to declare.

References

1. Chawla LS, Eggers PW, Star RA, and Kimmel PL. Acute kidney injury and chronic kidney disease as interconnected syndromes. *N Engl J Med.* 2014;371(1):58-66.
2. Susantitaphong P, Cruz DN, Cerda J, Abulfaraj M, Alqahtani F, Koulouridis I, et al. World incidence of AKI: a meta-analysis. *Clin J Am Soc Nephrol.* 2013;8(9):1482-93. doi: 10.2215/CJN.00710113. Epub 2013 Jun 6.
3. Bedford M, Farmer C, Levin A, Ali T, and Stevens P. Acute kidney injury and CKD: chicken or egg? *Am J Kidney Dis.* 2012;59(4):485-91. doi: 10.1053/j.ajkd.2011.09.010.
4. Ishani A, Xue JL, Himmelfarb J, Eggers PW, Kimmel PL, Molitoris BA, et al. Acute kidney injury increases risk of ESRD among elderly. *J Am Soc Nephrol.* 2009;20(1):223-8. doi: 10.1681/ASN.2007080837. Epub 2008 Nov 19.
5. Molitoris BA. Therapeutic translation in acute kidney injury: the epithelial/endothelial axis. *J Clin Invest.* 2014;124(6):2355-63. doi: 10.1172/JCI72269. Epub 2014 Jun 2.

6. Cavaille-Coll M, Bala S, Velidedeoglu E, Hernandez A, Archdeacon P, Gonzalez G, et al. Summary of FDA workshop on ischemia reperfusion injury in kidney transplantation. *Am J Transplant.* 2013;13(5):1134-48.
7. Lechevallier E, Dussol B, Luccioni A, Thirion X, Vacher-Copomat H, Jaber K, et al. Posttransplantation acute tubular necrosis: risk factors and implications for graft survival. *Am J Kidney Dis.* 1998;32(6):984-91.
8. Irish WD, McCollum DA, Tesi RJ, Owen AB, Brennan DC, Bailly JE, et al. Nomogram for predicting the likelihood of delayed graft function in adult cadaveric renal transplant recipients. *J Am Soc Nephrol.* 2003;14(11):2967-74.
9. Amdur RL, Chawla LS, Amodeo S, Kimmel PL, and Palant CE. Outcomes following diagnosis of acute renal failure in U.S. veterans: focus on acute tubular necrosis. *Kidney Int.* 2009;76(10):1089-97. doi: 10.38/ki.2009.332. Epub Sep 9.
10. Lo LJ, Go AS, Chertow GM, McCulloch CE, Fan D, Ordonez JD, et al. Dialysis-requiring acute renal failure increases the risk of progressive chronic kidney disease. *Kidney Int.* 2009;76(8):893-9. doi: 10.1038/ki.2009.289. Epub Jul 29.
11. Yarlagadda SG, Coca SG, Formica RN, Poggio ED, and Parikh CR. Association between delayed graft function and allograft and patient survival: a systematic review and meta-analysis. *Nephrol Dial Transpl.* 2009;24(3):1039-47.
12. Legendre C, Canaud G, and Martinez F. Factors influencing long-term outcome after kidney transplantation. *Transpl Int.* 2014;27(1):19-27.
13. Linkermann A, Chen G, Dong G, Kunzendorf U, Krautwald S, and Dong Z. Regulated cell death in AKI. *J Am Soc Nephrol.* 2014;25(12):2689-701.
14. Sharfuddin AA, and Molitoris BA. Pathophysiology of ischemic acute kidney injury. *Nat Rev Nephrol.* 2011;7(4):189-200. doi: 10.1038/nrneph.2011.16. Epub Mar 1.
15. Basile DP. The endothelial cell in ischemic acute kidney injury: implications for acute and chronic function. *Kidney Int.* 2007;72(2):151-6. Epub 2007 May 2.
16. Basile DP, Friedrich JL, Spahic J, Knipe N, Mang H, Leonard EC, et al. Impaired endothelial proliferation and mesenchymal transition contribute to vascular rarefaction following acute kidney injury. *Am J Physiol Renal Physiol.* 2011;300(3):F721-33. doi: 10.1152/ajprenal.00546.2010. Epub 2010 Dec 1.
17. Horbelt M, Lee SY, Mang HE, Knipe NL, Sado Y, Kribben A, et al. Acute and chronic microvascular alterations in a mouse model of ischemic acute kidney injury. *Am J Physiol Renal Physiol.* 2007;293(3):F688-95. Epub 2007 Jul 11.
18. Basile DP, Donohoe DL, Roethe K, and Mattson DL. Chronic renal hypoxia after acute ischemic injury: effects of L-arginine on hypoxia and secondary damage. *Am J Physiol Renal Physiol.* 2003;284(2):F338-48. Epub 2002 Oct 1.
19. Basile DP, Donohoe D, Roethe K, and Osborn JL. Renal ischemic injury results in permanent damage to peritubular capillaries and influences long-term function. *Am J Physiol Renal Physiol.* 2001;281(5):F887-99.
20. Basile DP, and Yoder MC. Renal endothelial dysfunction in acute kidney ischemia reperfusion injury. *Cardiovasc Hematol Disord Drug Targets.* 2014;14(1):3-14.
21. Steegh FM, Gelens MA, Nieman FH, van Hooff JP, Cleutjens JP, van Suylen RJ, et al. Early loss of peritubular capillaries after kidney transplantation. *J Am Soc Nephrol.* 2011;22(6):1024-9. doi: 10.681/ASN.2010050531. Epub 2011 May 12.
22. Ehling J, Babickova J, Gremse F, Klinkhammer BM, Baetke S, Knuechel R, et al. Quantitative Micro-Computed Tomography Imaging of Vascular Dysfunction in

548 Progressive Kidney Diseases. *J Am Soc Nephrol.* 2016;27(2):520-32. doi:
549 10.1681/ASN.2015020204. Epub 2015 Jul 20.
550 23. Babickova J, Klinkhammer BM, Buhl EM, Djudjaj S, Hoss M, Heymann F, et al.
551 Regardless of etiology, progressive renal disease causes ultrastructural and functional
552 alterations of peritubular capillaries. *Kidney Int.* 2017;91(1):70-85. doi:
553 10.1016/j.kint.2016.07.038. Epub Sep 24.
554 24. Menshikh A, Scarfe L, Delgado R, Finney C, Zhu Y, Yang H, et al. Capillary rarefaction
555 is more closely associated with CKD progression after cisplatin, rhabdomyolysis, and
556 ischemia-reperfusion-induced AKI than renal fibrosis. *Am J Physiol Renal Physiol.*
557 2019;317(5):F1383-F97.
558 25. Zhang X, Zheng X, Sun H, Feng B, Chen G, Vladau C, et al. Prevention of renal
559 ischemic injury by silencing the expression of renal caspase 3 and caspase 8.
560 *Transplantation.* 2006;82(12):1728-32.
561 26. Yang B, Lan S, Dieude M, Sabo-Vatasescu JP, Karakeussian-Rimbaud A, Turgeon J, et
562 al. Caspase-3 Is a Pivotal Regulator of Microvascular Rarefaction and Renal Fibrosis
563 after Ischemia-Reperfusion Injury. *J Am Soc Nephrol.* 2018;29(7):1900-16.
564 27. Yang B, Dieude M, Hamelin K, Henault-Rondeau M, Patey N, Turgeon J, et al. Anti-
565 LG3 Antibodies Aggravate Renal Ischemia-Reperfusion Injury and Long-Term Renal
566 Allograft Dysfunction. *American journal of transplantation : official journal of the*
567 *American Society of Transplantation and the American Society of Transplant Surgeons.*
568 2016;16(12):3416-29.
569 28. Langenberg C, Gobe G, Hood S, May CN, and Bellomo R. Renal histopathology during
570 experimental septic acute kidney injury and recovery. *Crit Care Med.* 2014;42(1):e58-67.
571 29. Chow BSM, and Allen TJ. Mouse Models for Studying Diabetic Nephropathy. *Curr*
572 *Protoc Mouse Biol.* 2015;5(2):85-94.
573 30. Racusen LC, Solez K, Colvin RB, Bonsib SM, Castro MC, Cavallo T, et al. The Banff 97
574 working classification of renal allograft pathology. *Kidney Int.* 1999;55(2):713-23.
575 31. Sirois I, Groleau J, Pallet N, Brassard N, Hamelin K, Londono I, et al. Caspase activation
576 regulates the extracellular export of autophagic vacuoles. *Autophagy.* 2012;8(6):927-37.
577 32. Ehling J, Babickova J, Gremse F, Klinkhammer BM, Baetke S, Knuechel R, et al.
578 Quantitative Micro-Computed Tomography Imaging of Vascular Dysfunction in
579 Progressive Kidney Diseases. *J Am Soc Nephrol.* 2016;27(2):520-32.
580 33. Ghanavati S, Yu LX, Lerch JP, and Sled JG. A perfusion procedure for imaging of the
581 mouse cerebral vasculature by X-ray micro-CT. *J Neurosci Methods.* 2014;221:70-7.
582 34. Babickova J, Klinkhammer BM, Buhl EM, Djudjaj S, Hoss M, Heymann F, et al.
583 Regardless of etiology, progressive renal disease causes ultrastructural and functional
584 alterations of peritubular capillaries. *Kidney Int.* 2017;91(1):70-85.
585 35. Ferrero ME. In vivo vascular leakage assay. *Methods Mol Med.* 2004;98:191-8.
586 36. Westhorpe CL, Bayard JE, O'Sullivan KM, Hall P, Cheng Q, Kitching AR, et al. In Vivo
587 Imaging of Inflamed Glomeruli Reveals Dynamics of Neutrophil Extracellular Trap
588 Formation in Glomerular Capillaries. *Am J Pathol.* 2017;187(2):318-31.
589 37. Molitoris BA. Therapeutic translation in acute kidney injury: the epithelial/endothelial
590 axis. *J Clin Invest.* 2014;124(6):2355-63.
591 38. Basile DP. The case for capillary rarefaction in the AKI to CKD progression: insights
592 from multiple injury models. *Am J Physiol Renal Physiol.* 2019;317(5):F1253-F4.

39. Zager RA, Johnson ACM, Andress D, and Becker K. Progressive endothelin-1 gene activation initiates chronic/end-stage renal disease following experimental ischemic/reperfusion injury. *Kidney International.* 2013;84(4):703-12.
40. Basile DP, Donohoe D, Roethe K, and Osborn JL. Renal ischemic injury results in permanent damage to peritubular capillaries and influences long-term function. *Am J Physiol Renal Physiol.* 2001;281(5):F887-99.
41. Yang L, Besschetnova TY, Brooks CR, Shah JV, and Bonventre JV. Epithelial cell cycle arrest in G2/M mediates kidney fibrosis after injury. *Nat Med.* 2010;16(5):535-43, 1p following 143.
42. Grgic I, Campanholle G, Bijol V, Wang C, Sabbisetti VS, Ichimura T, et al. Targeted proximal tubule injury triggers interstitial fibrosis and glomerulosclerosis. *Kidney Int.* 2012;82(2):172-83.
43. Fu Y, Tang C, Cai J, Chen G, Zhang D, and Dong Z. Rodent models of AKI-CKD transition. *Am J Physiol Renal Physiol.* 2018;315(4):F1098-F106.
44. Skrypnyk NI, Harris RC, and de Caestecker MP. Ischemia-reperfusion Model of Acute Kidney Injury and Post Injury Fibrosis in Mice. *Jove-J Vis Exp.* 2013(78).
45. Forni LG, Darmon M, Ostermann M, Oudemans-van Straaten HM, Pettila V, Prowle JR, et al. Renal recovery after acute kidney injury. *Intensive Care Med.* 2017;43(6):855-66.
46. Rippe C, Rippe A, Larsson A, Asgeirsson D, and Rippe B. Nature of glomerular capillary permeability changes following acute renal ischemia-reperfusion injury in rats. *Am J Physiol Renal Physiol.* 2006;291(6):F1362-8.
47. Picken M, Long J, Williamson GA, and Polichnowski AJ. Progression of Chronic Kidney Disease After Acute Kidney Injury: Role of Self-Perpetuating Versus Hemodynamic-Induced Fibrosis. *Hypertension.* 2016;68(4):921-8.
48. Sutton TA, Mang HE, Campos SB, Sandoval RM, Yoder MC, and Molitoris BA. Injury of the renal microvascular endothelium alters barrier function after ischemia. *Am J Physiol Renal Physiol.* 2003;285(2):F191-8.
49. Olof P, Hellberg A, Kallskog O, and Wolgast M. Red cell trapping and postischemic renal blood flow. Differences between the cortex, outer and inner medulla. *Kidney Int.* 1991;40(4):625-31.
50. Sutton TA. Alteration of microvascular permeability in acute kidney injury. *Microvasc Res.* 2009;77(1):4-7.
51. Ko GJ, Grigoryev DN, Linfert D, Jang HR, Watkins T, Cheadle C, et al. Transcriptional analysis of kidneys during repair from AKI reveals possible roles for NGAL and KIM-1 as biomarkers of AKI-to-CKD transition. *Am J Physiol Renal Physiol.* 2010;298(6):F1472-83.
52. Schaub JA, and Parikh CR. Biomarkers of acute kidney injury and associations with short- and long-term outcomes. *F1000Res.* 2016;5.
53. Chou YH, Huang TM, and Chu TS. Novel insights into acute kidney injury-chronic kidney disease continuum and the role of renin-angiotensin system. *Journal of the Formosan Medical Association.* 2017;116(9):652-9.
54. Devarajan P. The Use of Targeted Biomarkers for Chronic Kidney Disease. *Adv Chronic Kidney D.* 2010;17(6):469-79.
55. Sirois I, Raymond MA, Brassard N, Cailhier JF, Fedjaev M, Hamelin K, et al. Caspase-3-dependent export of TCTP: a novel pathway for antiapoptotic intercellular communication. *Cell death and differentiation.* 2011;18(3):549-62.

56. Futrakul N, and Futrakul P. Biomarker for early renal microvascular and diabetic kidney diseases. *Ren Fail.* 2017;39(1):505-11.
57. Cardinal H, Dieude M, and Hebert MJ. Endothelial Dysfunction in Kidney Transplantation. *Front Immunol.* 2018;9:1130.
58. Dieude M, Bell C, Turgeon J, Beillevaire D, Pomerleau L, Yang B, et al. The 20S proteasome core, active within apoptotic exosome-like vesicles, induces autoantibody production and accelerates rejection. *Sci Transl Med.* 2015;7(318):318ra200.
59. Chade AR. Small Vessels, Big Role: Renal Microcirculation and Progression of Renal Injury. *Hypertension.* 2017;69(4):551-63.
60. Ohnishi Y, Yasudo H, Suzuki Y, Furuta T, Matsuguma C, Azuma Y, et al. Circulating endothelial glycocalyx components as a predictive marker of coronary artery lesions in Kawasaki disease. *Int J Cardiol.* 2019;292:236-40.
61. Powell TC, Powell SL, Allen BK, Griffin RL, Warnock DG, and Wang HE. Association of inflammatory and endothelial cell activation biomarkers with acute kidney injury after sepsis. *Springerplus.* 2014;3:207.
62. Chironi GN, Boulanger CM, Simon A, Dignat-George F, Freyssinet JM, and Tedgui A. Endothelial microparticles in diseases. *Cell Tissue Res.* 2009;335(1):143-51.
63. Xu J, Buchwald JE, and Martins PN. Review of Current Machine Perfusion Therapeutics for Organ Preservation. *Transplantation.* 2020;104(9):1792-803.
64. Ferrari RS, and Andrade CF. Oxidative Stress and Lung Ischemia-Reperfusion Injury. *Oxidative Medicine and Cellular Longevity.* 2015;2015:1-14.
65. Feltes CM, Hassoun HT, Lie ML, Cheadle C, and Rabb H. Pulmonary endothelial cell activation during experimental acute kidney injury. *Shock.* 2011;36(2):170-6.
66. Gonzalez LM, Moeser AJ, and Blikslager AT. Animal models of ischemia-reperfusion-induced intestinal injury: progress and promise for translational research. *Am J Physiol Gastrointest Liver Physiol.* 2015;308(2):G63-75.
67. Homsi E, Janino P, and de Faria JB. Role of caspases on cell death, inflammation, and cell cycle in glycerol-induced acute renal failure. *Kidney Int.* 2006;69(8):1385-92.
68. Nydam TL, Plenter R, Jain S, Lucia S, and Jani A. Caspase Inhibition During Cold Storage Improves Graft Function and Histology in a Murine Kidney Transplant Model. *Transplantation.* 2018;102(9):1487-95.
69. Zhang X, Zheng X, Sun H, Feng B, Chen G, Vladau C, et al. Prevention of renal ischemic injury by silencing the expression of renal caspase 3 and caspase 8. *Transplantation.* 2006;82(12):1728-32.
70. Yang C, Zhao T, Zhao Z, Jia Y, Li L, Zhang Y, et al. Serum-stabilized naked caspase-3 siRNA protects autotransplant kidneys in a porcine model. *Mol Ther.* 2014;22(10):1817-28.
71. Baskin-Bey ES, Washburn K, Feng S, Oltersdorf T, Shapiro D, Huyghe M, et al. Clinical Trial of the Pan-Caspase Inhibitor, IDN-6556, in Human Liver Preservation Injury. *American journal of transplantation : official journal of the American Society of Transplantation and the American Society of Transplant Surgeons.* 2007;7(1):218-25.

Figure legends:

Figure 1: Caspase-3 deficient mice show reduced long-term tubular and microvascular injury after renal IRI and better-preserved renal function after severe IRI. (A) Serum creatinine levels in wild-type and caspase-$3^{-/-}$ (KO) mice at baseline (pre-operation), and 1, 2, 7 and 21 days post 30 min and 60 min IRI. (B) Left panel: Representative haematoxylin and eosin (H&E) stained renal sections showing tubular injury from wild-type and caspase-$3^{-/-}$ mice at 21 days post 60 min IRI. Black arrow: polynuclear neutrophil; green arrow: cast formation; blue arrow: tubular dilation (magnification 200X and 400X). Right panel: Mean tubular injury scores of ten randomly chosen high-power fields in mice renal cortical sections at pre-operation and post-IRI at 1, 2, 7 and 21 days from wild-type and caspase-$3^{-/-}$ mice that underwent 30 min and 60 min IRI. (C) Left panel: Representative H&E-stained murine renal sections showing rouleaux formation at 21 days post 60 min IRI (magnification 200X and 400 X). Red arrow: rouleaux formation (vascular congestion). Right panel: Quantification of rouleaux formation in H&E-stained renal cortical sections at pre-operation and post-IRI at 1, 2, 7 and 21 days from wild-type and caspase-$3^{-/-}$ mice that underwent 30 min and 60 min IRI. Scale bar = 50 μm (magnification 200X), scale bar = 100 μm (magnification 400X). Values are mean ± SEM. * $P < 0.05$ between group.

Figure 2: Caspase-3 deficiency preserves the integrity of peritubular capillaries post-IRI. (A) Upper panel: Representative images of MECA-32 immunohistochemistry in the whole kidney and renal cortical-medullary junction from wild-type and caspase-$3^{-/-}$ mice that underwent 60 min IRI and were sacrificed 21 days post-IRI or sham-operation (magnification 200X). Lower panel: Quantification of MECA-32 positive peritubular capillary (PTC) in murine renal cortical-medullary junction sections at 21 days post 30 min and 60 min IRI or sham group. (B) Left panel: Representative images of MECA-32 immunohistochemistry staining within glomeruli from wild-type and caspase-$3^{-/-}$ mice that underwent 60 min IRI and were sacrificed 21 days post-IRI or sham-operation (magnification 200X). Right panel: Quantification of MECA-32 positive glomeruli in murine renal sections at 21 days post 30 min and 60 min IRI or sham group. Scale bar = 50 μm. Values are mean ± SEM.* $P < 0.05$ between group. # $P < 0.05$ compared to WT or KO SHAM.

Figure 3: Caspase-3 deficiency prevents endothelial apoptosis after severe IRI. (A-C): Representative electron micrographs of PTC from wild-type mice that underwent 60 min IRI and sacrificed 21 days post-IRI. (D-F): Representative EM images of PTC from caspase-3$^{-/-}$ mice that underwent 60 min IRI and sacrificed 21 days post-IRI. Blue arrow: apoptotic bodies; red arrow: apoptotic exosome-like vesicles; yellow arrow: nuclear condensation; black arrow: capillary endothelium fenestration; scale bar = 2 μm.

Figure 4: Caspase-3 deficiency prevents microvascular rarefaction of peritubular capillaries in mild and severe forms of IRI. (A) Representative microCT 3D reconstruction images of whole renal microvasculature from wild-type and caspase-3$^{-/-}$ mice that underwent 30 min and 60 min IRI and were sacrificed at 21 days post-IRI or pre-operation. Terminal capillaries in the kidney are labeled as green dots, scale bar = 1000 μm. (B) Quantification of total renal blood vessel volume from wild-type and caspase-3$^{-/-}$ mice at 21 days post 30 min and 60 min IRI or sham-operation. (C) Quantification of renal terminal capillary number from wild-type and caspase-3$^{-/-}$ mice at 21 days post 30 min and 60 min IRI or sham-operation. Values are mean ± SEM. * $P < 0.05$ between group. # $P < 0.05$ compared to WT or KO SHAM.

Figure 5: Caspase-3 deficient mice show reduced long-term endothelial permeability disturbances after mild and severe IRI. (A) Representative intra-vital live images showing renal microvascular endothelial permeability and perfusion from wild-type and caspase-3$^{-/-}$ mice that underwent 30 min and 60 min IRI and were sacrificed 21 days post-IRI. Green channel: fluorescein isothiocyanate-labeled dextran (2000 kDa); red channel: Evans Blue dye; white arrow: peritubular capillary (PTC) permeability depicted by Evans Blue leaking, scale bar = 50 μm. (B) Quantification of the length of non-perfused renal PTC from wild-type and caspase-3$^{-/-}$ mice at 21 days post 30 min and 60 min IRI. (C) Quantification of renal PTC perfusion ratio from wild-type and caspase-3$^{-/-}$ mice at 21 days post 30 min and 60 min IRI. (D) Left panel: Representative images of a retrieved ischemic kidney after Evans Blue perfusion from wild-type and caspase-3$^{-/-}$ mice that underwent 60 min IRI and were sacrificed 21 days post-IRI. Right panel: Quantification of renal *ex vivo* Evans Blue extravasation volume from wild-type and caspase-3$^{-/-}$ mice at 21 days post 30 min and 60 min IRI or

sham-operation. Values are mean ± SEM. * P < 0.05 between group. # P < 0.05 compared to WT or KO SHAM.

Figure 6: Caspase-3 deficiency attenuates long-term collagen deposition in peritubular capillary after mild and severe IRI. (A) Left panel: Representative images of Sirius Red staining within peritubular capillary (PTC) in renal cortical-medullary junction sections from wild-type and caspase-$3^{-/-}$ mice that underwent 60 min IRI and were sacrificed 21 days post-IRI, or sham-operation. Arrowheads show collagen deposition in PTC (magnification 200X), scale bar = 50 μm. Right panel: Quantification of Sirius Red positive area within PTC in murine renal cortical-medullary junction sections at pre-operation, sham-operation, and 21 days post 30 min and 60 min IRI. (B) Left panel: Representative Sirius Red positive glomeruli in renal cortical section from wild-type and caspase-$3^{-/-}$ mice that underwent 60 min IRI and were sacrificed 21 days post-IRI, or sham-operation (magnification 200X), scale bar = 50 μm. Right panel: Quantification of Sirius Red positive glomeruli in renal cortical section from wild-type and caspase-$3^{-/-}$ mice at pre-operation, sham-operation and 21 days post 30 min and 60 min IRI. (C) Representative electron micrographs of collagen deposition in PTC from wild-type and caspase-$3^{-/-}$ mice that underwent 60 min IRI and were sacrificed 21 days post-IRI (magnification 3200X), arrowhead: collagen deposition in PTC, scale bar = 2 μm. Values are mean ± SEM.* P < 0.05 between group. # P < 0.05 compared to WT or KO SHAM.

Figure 7: Caspase-3 deficient mice show reduced long-term renal fibrosis after mild and severe IRI. (A) Upper panel: Representative α-SMA immunohistochemistry staining in whole murine kidney section 21 days after 60 min IRI. Middle panel: Representative α-SMA immunohistochemistry staining within peritubular capillary (PTC) in renal cortical section at day 21 after 60 min IRI (magnification 200X), scale bar = 50 μm. Lower panel: Representative α-SMA immunohistochemistry staining within glomeruli in renal cortical section at day 21 after 60 min IRI (magnification 200X), scale bar = 50 μm. (B) Quantification of α-SMA positive PTC in renal cortical sections from wild-type and caspase-$3^{-/-}$ mice at 21 days post 30 min and 60 min IRI. (C) Quantification of α-SMA positive glomeruli in renal cortical sections from wild-type and caspase-$3^{-/-}$ mice at 21 days post 30 min and 60 min IRI. (D) Quantification of α-SMA positive cells in

764 macrovessels in renal sections from wild-type and caspase-$3^{-/-}$ mice at 21 days post 30 min and 60
765 min IRI. Values are mean ± SEM. * P < 0.05 between group. # P < 0.05 compared to WT or KO
766 SHAM.

767 **Figure 8 : Impact of caspase-3 on microvascular endothelial injury and renal fibrosis and**
768 **dysfunction post-IRI**. Microvascular injury induced by renal IRI increases disturbances in
769 microvascular permeability and microvascular rarefaction. It promotes secondary tubular injury,
770 collagen deposition and myofibroblast differentiation, which result in long-term renal dysfunction and
771 renal interstitial fibrosis. Caspase-3 is a pivotal regulator of renal dysfunction as its deficiency largely
772 prevents the above pathophysiological changes.
773
774
775
776
777

Supplementary Figure legends:

Supplementary Figure 1: Caspase-3 deficiency ameliorates long-term renal tubular injury and microvascular injury after mild IRI. (A) Tubular injury in representative renal sections from wild-type and caspase-$3^{-/-}$ mice at day 21 post 30 min of IRI and stained with haematoxylin and eosin (H&E). (magnifications 200X and 400X). (B) Representative H&E-stained renal sections showing rouleaux formation at day 21 post 30 min of IRI (magnifications 200X and 400X). Scale bar = 50 µm (magnification 200X), scale bar = 100 µm (magnification 400X).

Supplementary Figure 2: Description of multiple morphologies in MECA-32 immunohistochemistry staining in peritubular capillaries (PTCs). Upper panel: Representative images of MECA-32 immunohistochemistry (magnification 200X), scale bar = 50 µm. Lower panel: a: Capillary lumen is clearly stained; b: Capillary lumen is weakly stained; c: Capillary lumen is weakly stained, but the structural outline is visible; d: Smaller positive capillary; e: Capillary lumen is invisible, but the longitudinal axis is visible; f: Capillary lumen is visible, with cellular circulation inside.

Supplementary Figure 3: Caspase-3 deficiency prevents endothelial apoptosis post severe IRI. (A) Representative images of caspase-3 immunohistochemistry from wild-type and caspase-$3^{-/-}$ mice that underwent 60 min IRI (magnification 200X). Arrow: caspase-3 positive endothelial-like cells. (B) Quantification of caspase-3 positive endothelial-like cells in PTC from wild-type mice and caspase-$3^{-/-}$ mice at 21 days post 60 min IRI. Scale bar = 50 µm. Values are mean ± SEM.* $P < 0.05$.

Supplementary Figure 4: Caspase-3 deficiency does not modulate long term renal glomerulosclerosis post severe IRI. (A) Representative photos of silver-stained renal sections showing glomerulosclerosis at day 21 post 60 min of IRI (magnification 200X). (B) Quantification of glomerulosclerosis in murine renal glomeruli at day 21 post 60 min of IRI, scale bar = 50 µm. Values are mean ± SEM.* $P < 0.05$.

Supplementary Figure 5: Intra-vital images of renal capillary perfusion in sham-operated mice. (A) Upper panel: intra-vital images of peritubular capillaries prior to Evans Blue injection and 30 seconds, 5 minutes, and 15 minutes post-injection in sham-operated WT mice. (B) Lower panel:

intra-vital images of peritubular capillaries prior to Evans Blue injection and 30 seconds, 5 minutes, and 15 minutes post-injection in sham-operated caspase-$3^{-/-}$ mice. Scale bar = 50 μm.

Supplementary Figure 6: Definitions of different types of renal capillaries in intra-vital live confocal imaging. (A) Definition and example of capillary segments quantification. (B) Definitions and examples of multiple types of renal peritubular capillaries (PTCs) post-IRI.

Supplementary Figure 7: Caspase-3 deficiency ameliorates tubular hypoxia after AKI. (A) Quantification of HIF-1α in murine renal cortical section at day 21 post 30 min and 60 min of IRI. (B) Quantification of HIF-1α at the cortical-medullary junction at day 21 post 30 min and 60 min of IRI. Values are mean ± SEM.* $P < 0.05$.

Video 1: Z stack image showing PTC leaking in WT mice at day 21 post IR for 60 min (zoom 3). Red area: Evans Blue leakage. Yellow/Green: Capillary. Blue: Tubules.

Video 2: Z stack image showing PTC leaking in caspase-$3^{-/-}$ mice at day 21 post IR for 60 min (zoom 3). Red area: Evans Blue leakage. Yellow/Green: Capillary. Blue: Tubules.

Video 3: Live imaging showing PTC perfusion in WT mice at day 21 post IR for 60 min (zoom1-zoom3). Red area: Evans Blue leakage . Yellow/Green: Capillary. Blue: Tubules.

Video 4: Live imaging showing PTC perfusion in caspase-$3^{-/-}$ mice at day 21 post IR for 60 min (zoom1-zoom3). Red area: Evans Blue leakage. Yellow/Green: Capillary. Blue: Tubules.

Video 5: Live imaging showing glomerular leakage in WT mice at day 21 post IR for 30 min (zoom 1). Red area: Evans Blue leakage. Yellow/Green: Capillary. Blue: Tubules. Star: Glomerular leakage of Evans Blue in tubular lumen.

Video 6: Live imaging showing PTC leakage and glomerular leakage in caspase-$3^{-/-}$ mice at day 21 post IR for 30 min (zoom 1). Red area: Evans Blue leakage. Yellow/Green: Capillary. Blue: Tubules. Arrow: PTC leakage of Evans Blue. Star: Glomerular leakage of Evans Blue in tubular lumen.

Video 7: Live imaging showing PTC leaking process (zoom 1). Red area: Evans Blue leakage. Yellow/Green: Capillary. Blue: Tubules. Arrow: PTC leakage of Evans Blue.

Video 8: Live imaging showing glomerular leaking process (zoom 3). Red area: Evans Blue leakage. Yellow/Green: Capillary. Blue: Tubules. Star: Glomerular leakage of Evans Blue in tubular lumen.

Video 9: Live imaging showing different renal PTCs definitions post-IRI (zoom 3). Arrowhead: non-perfused PTC; Arrow: perfused PTC without circulation; Star: PTC with normal circulation.

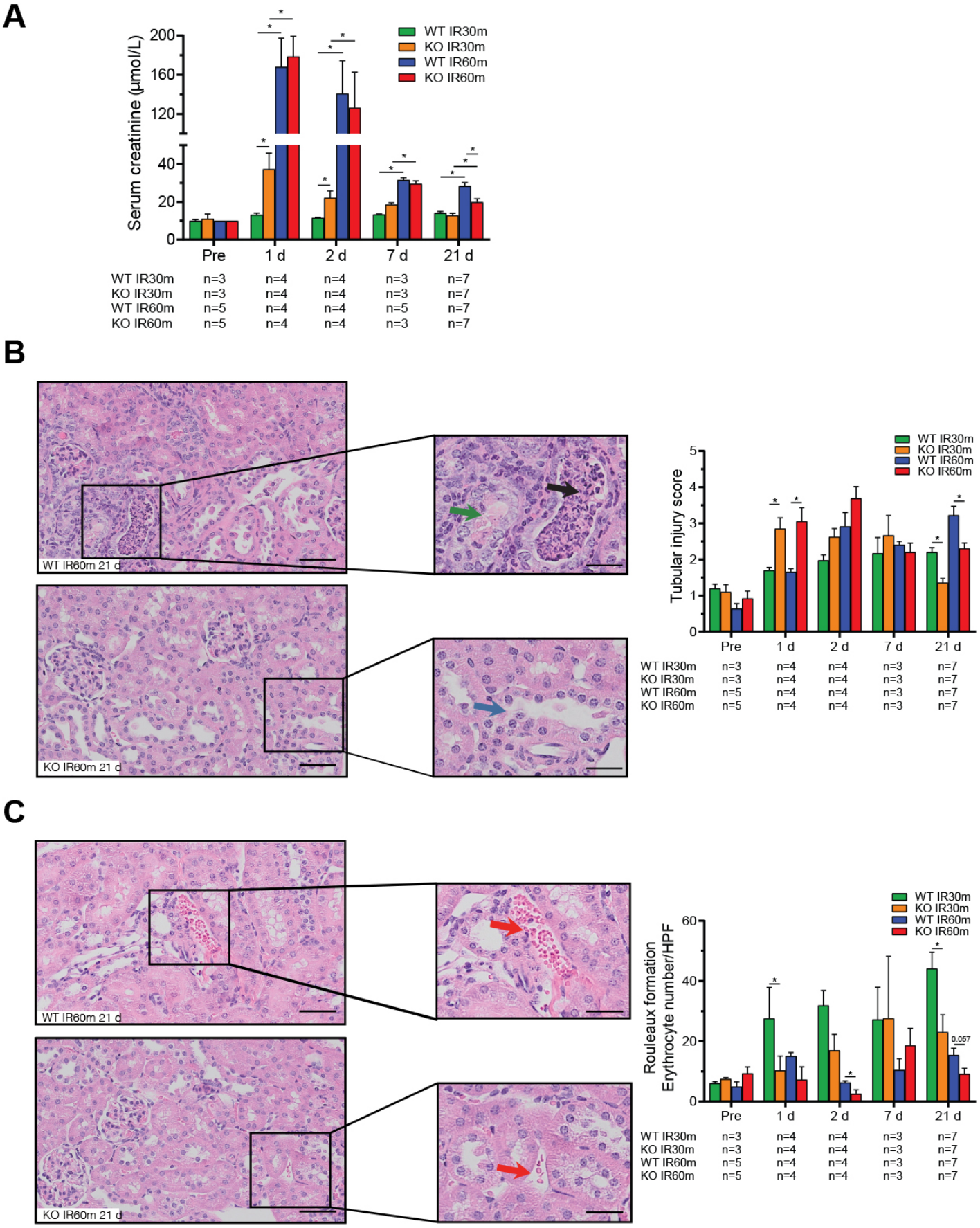

Figure 1: Caspase-3 deficient mice show reduced long-term tubular and microvascular injury after renal IRI and better-preserved renal function after severe IRI.

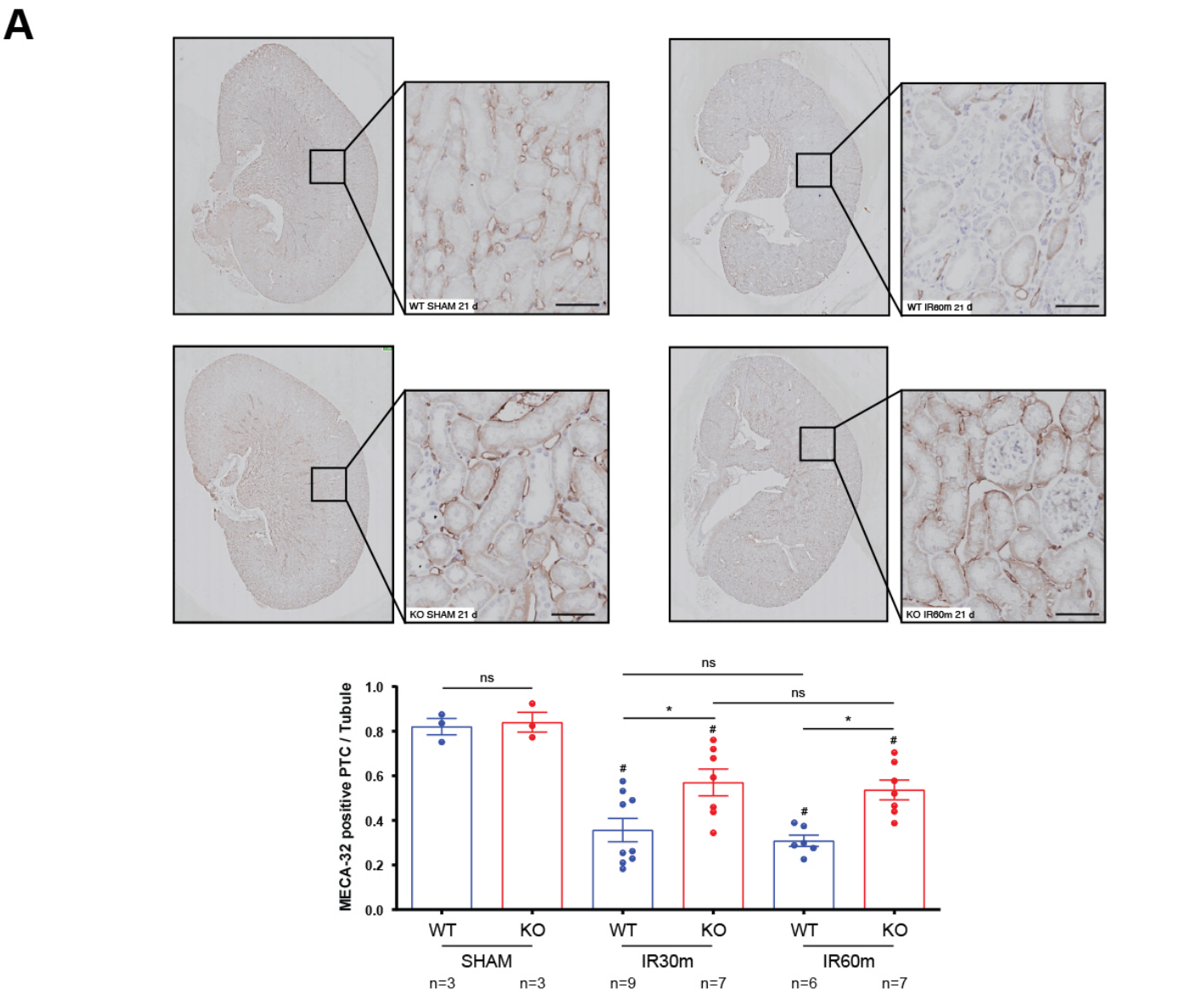

Figure 2: Caspase-3 deficiency preserves the integrity of peritubular capillaries post-IRI.

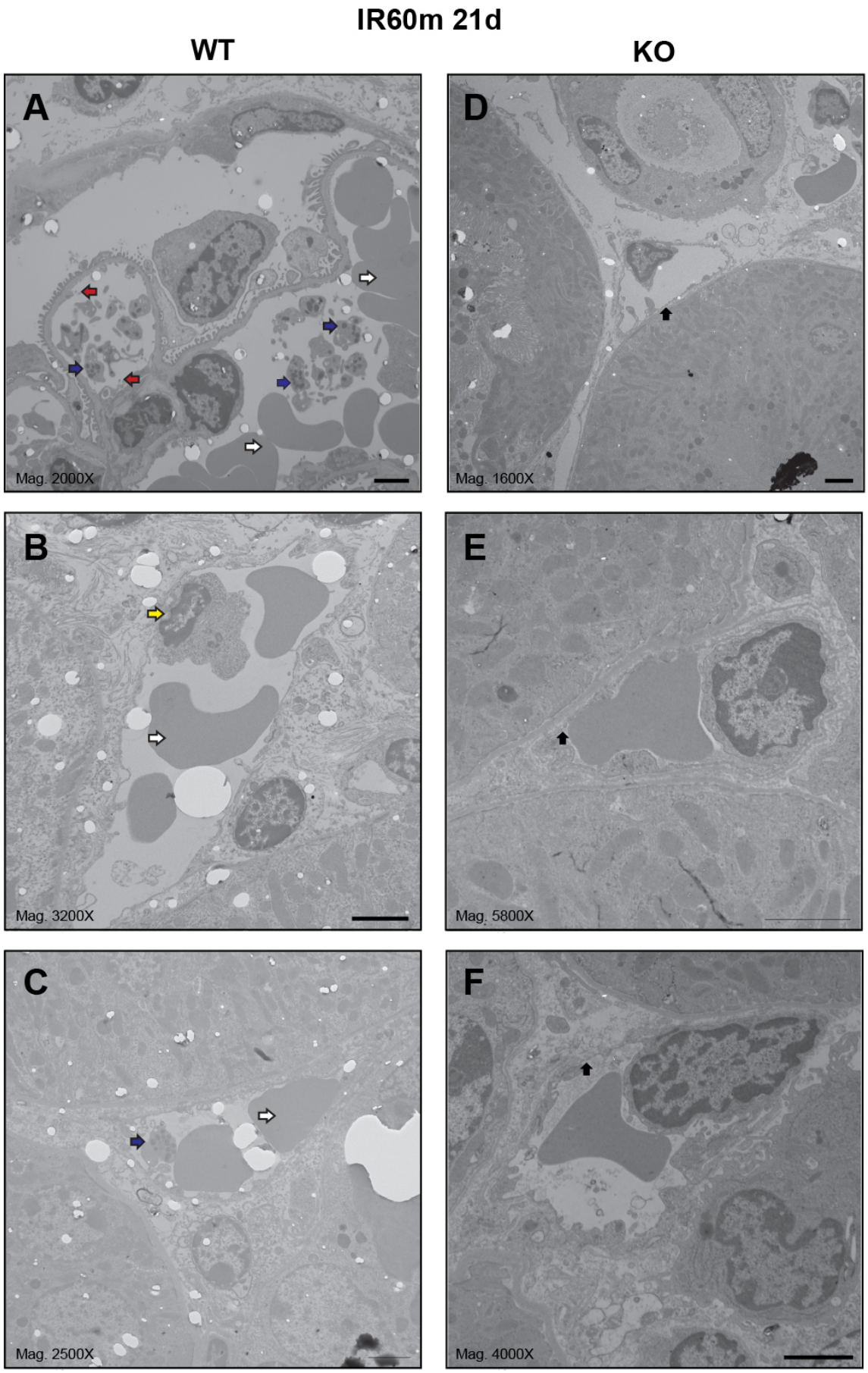

Figure 3: Caspase-3 deficiency prevents endothelial apoptosis post severe IRI.

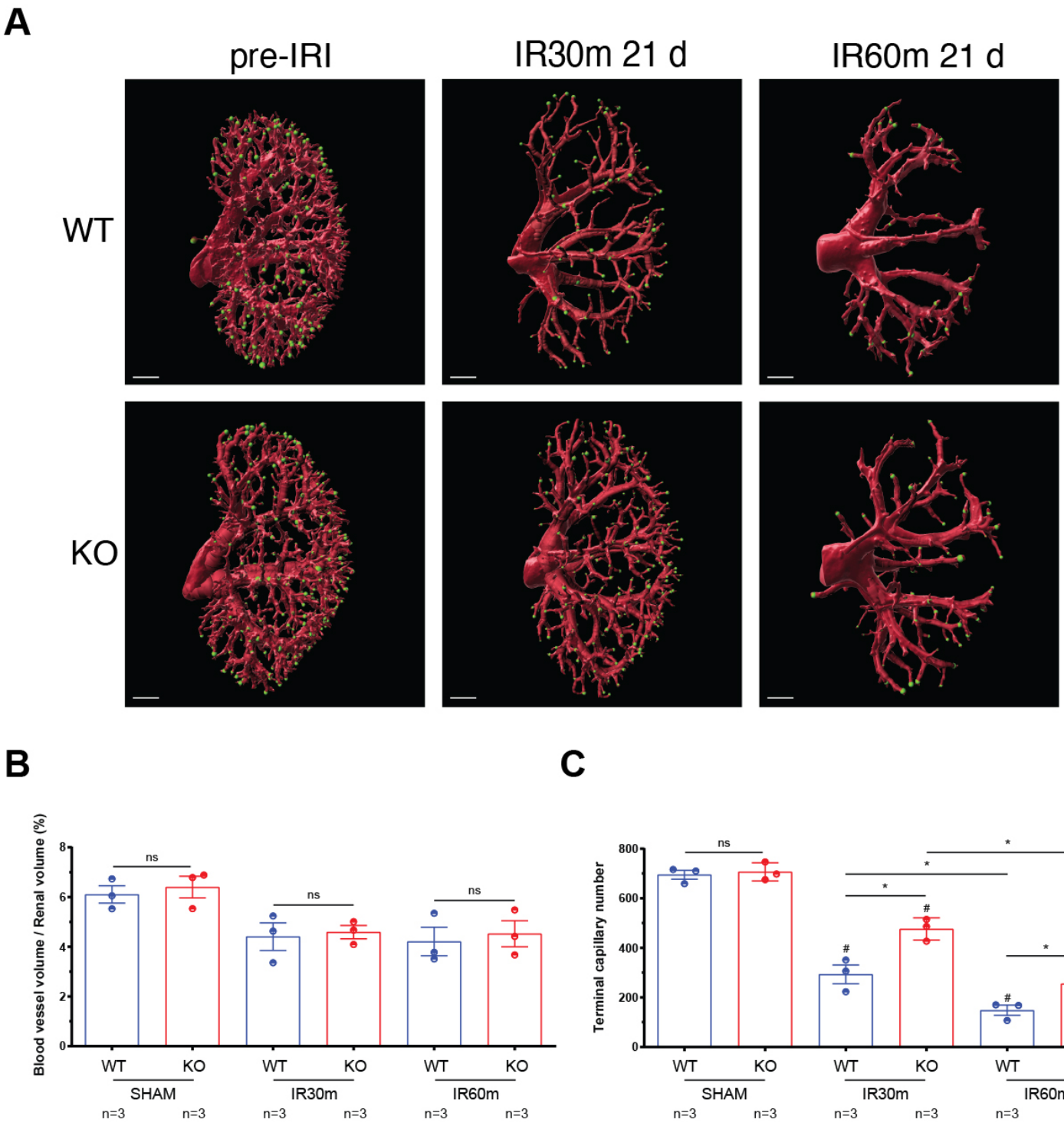

Figure 4: Caspase-3 deficiency prevents microvascular rarefaction of terminal capillary in mild and severe forms of IRI.

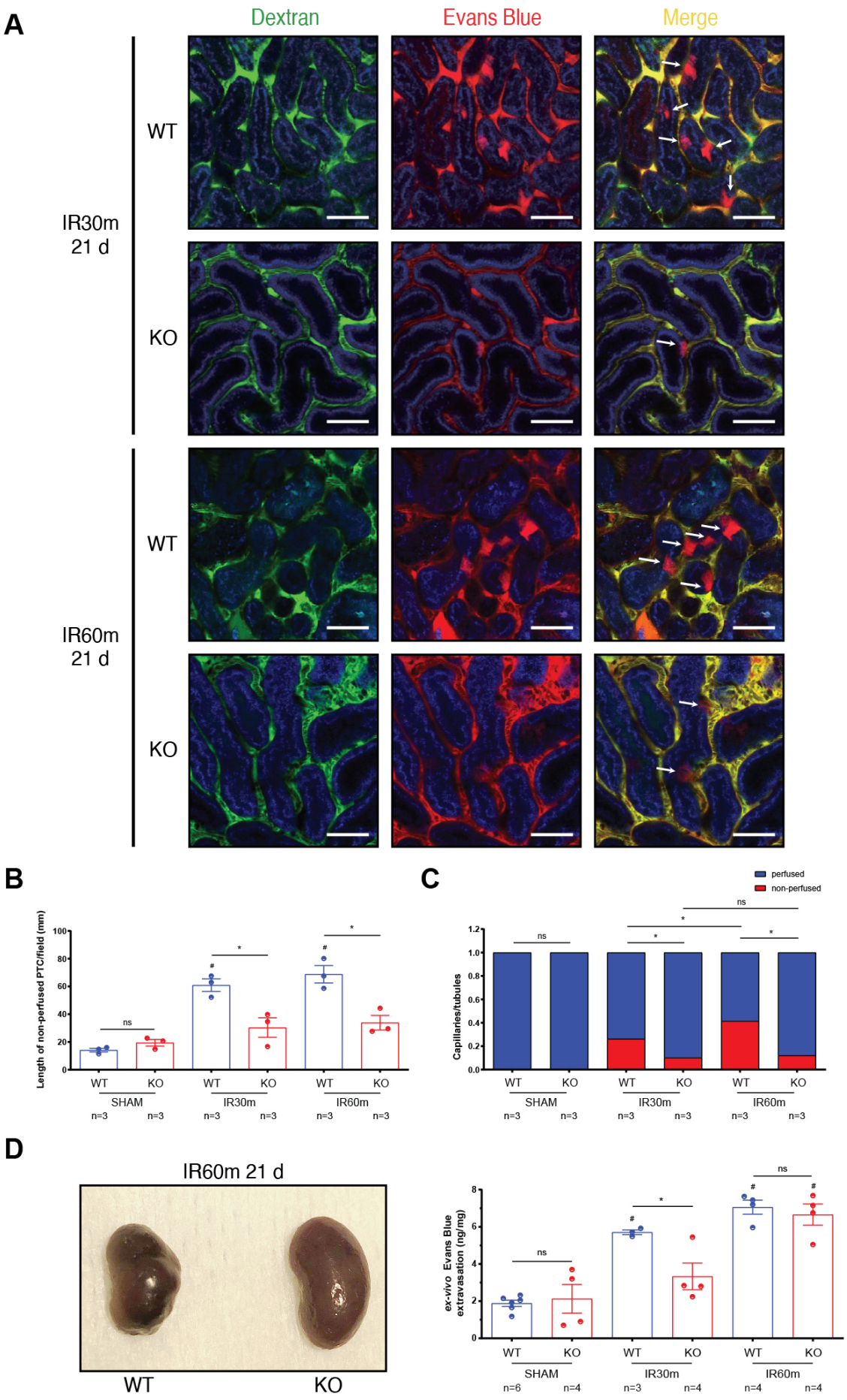

Figure 5: Caspase-3 deficient mice show reduced long-term endothelial permeability disturbances after mild and severe IRI.

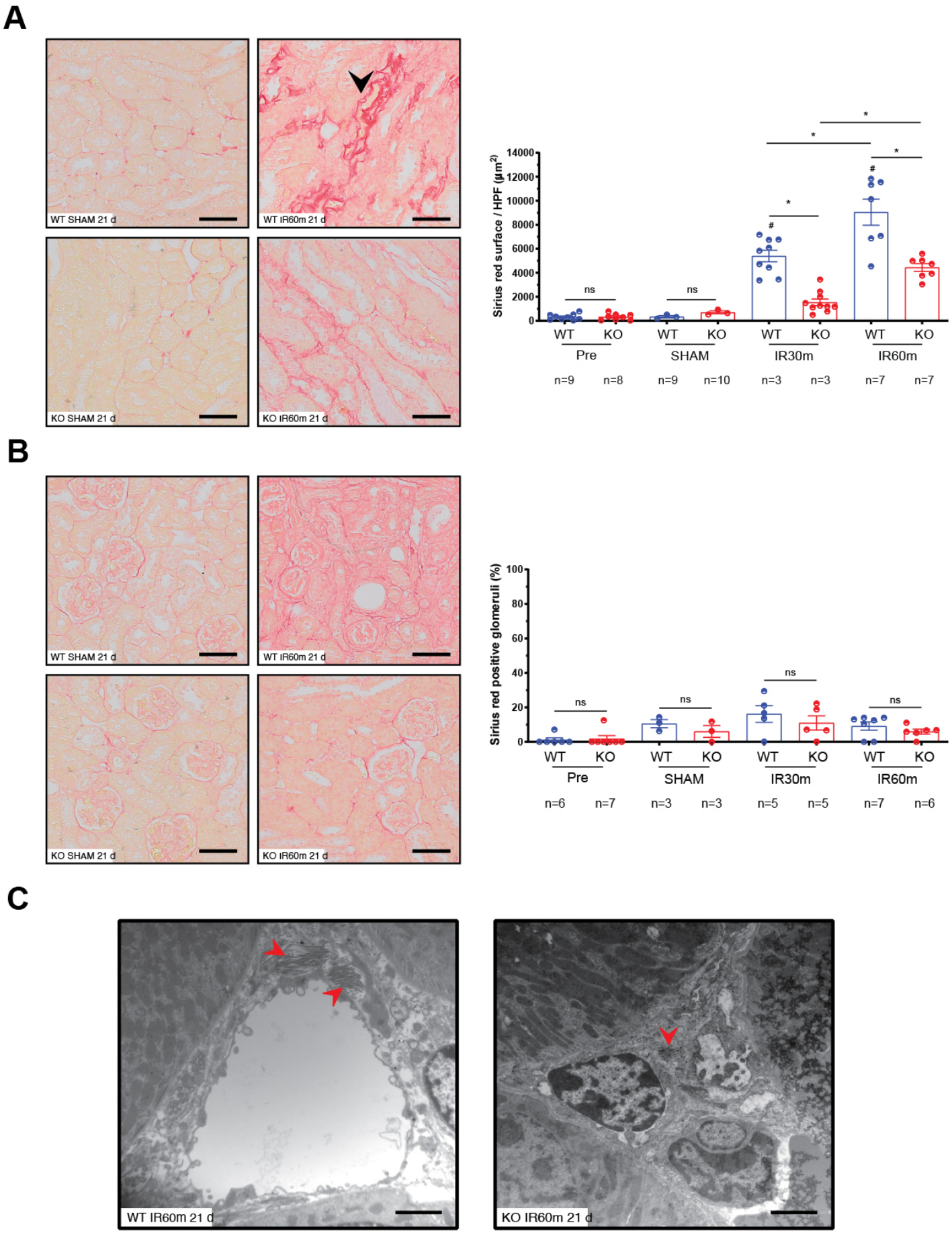

Figure 6: Caspase-3 deficiency attenuates long-term collagen deposition in peritubular capillary after mild and severe IRI.

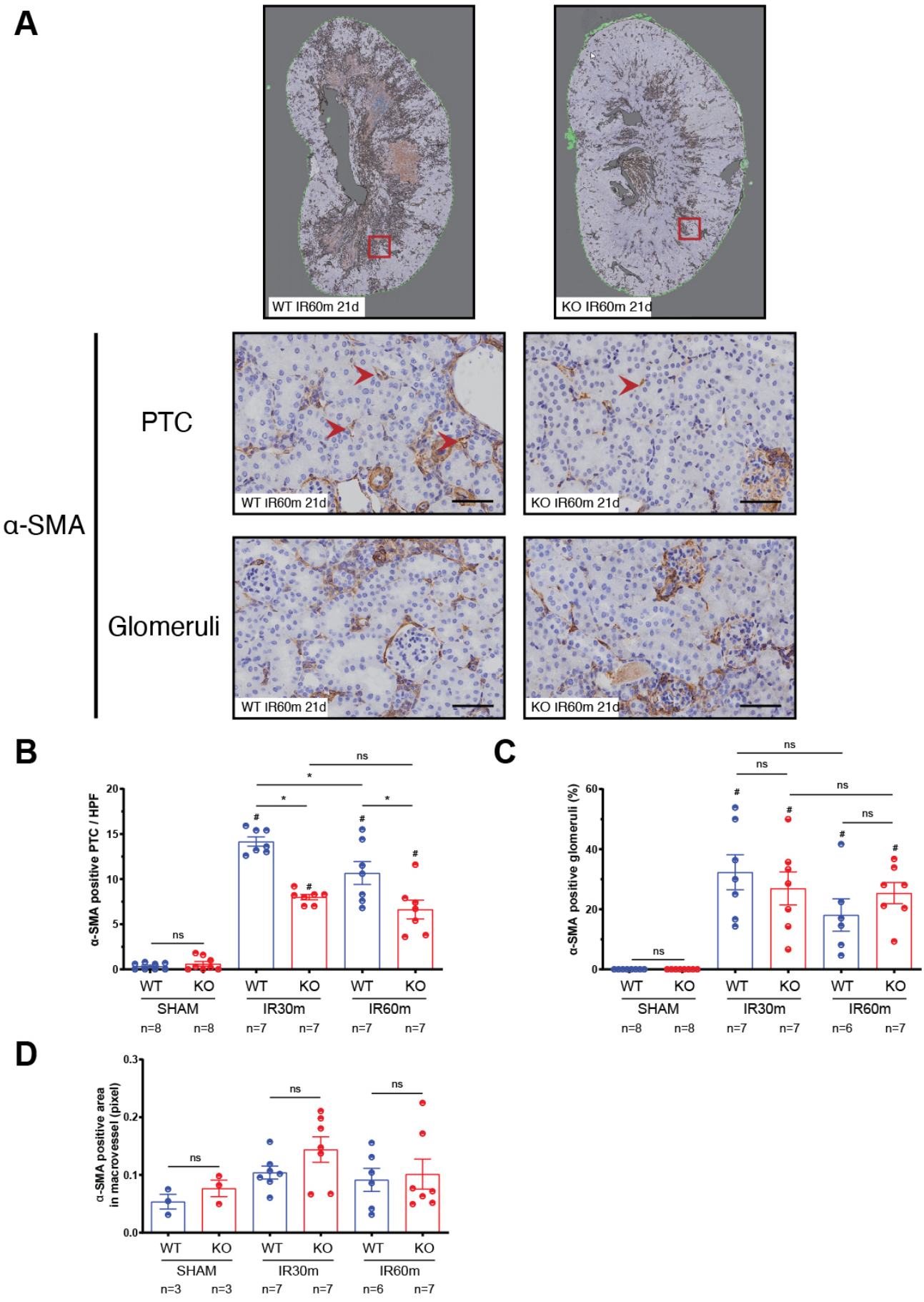

Figure 7: Caspase-3 deficient mice show reduced long-term renal fibrosis after mild and severe IRI.

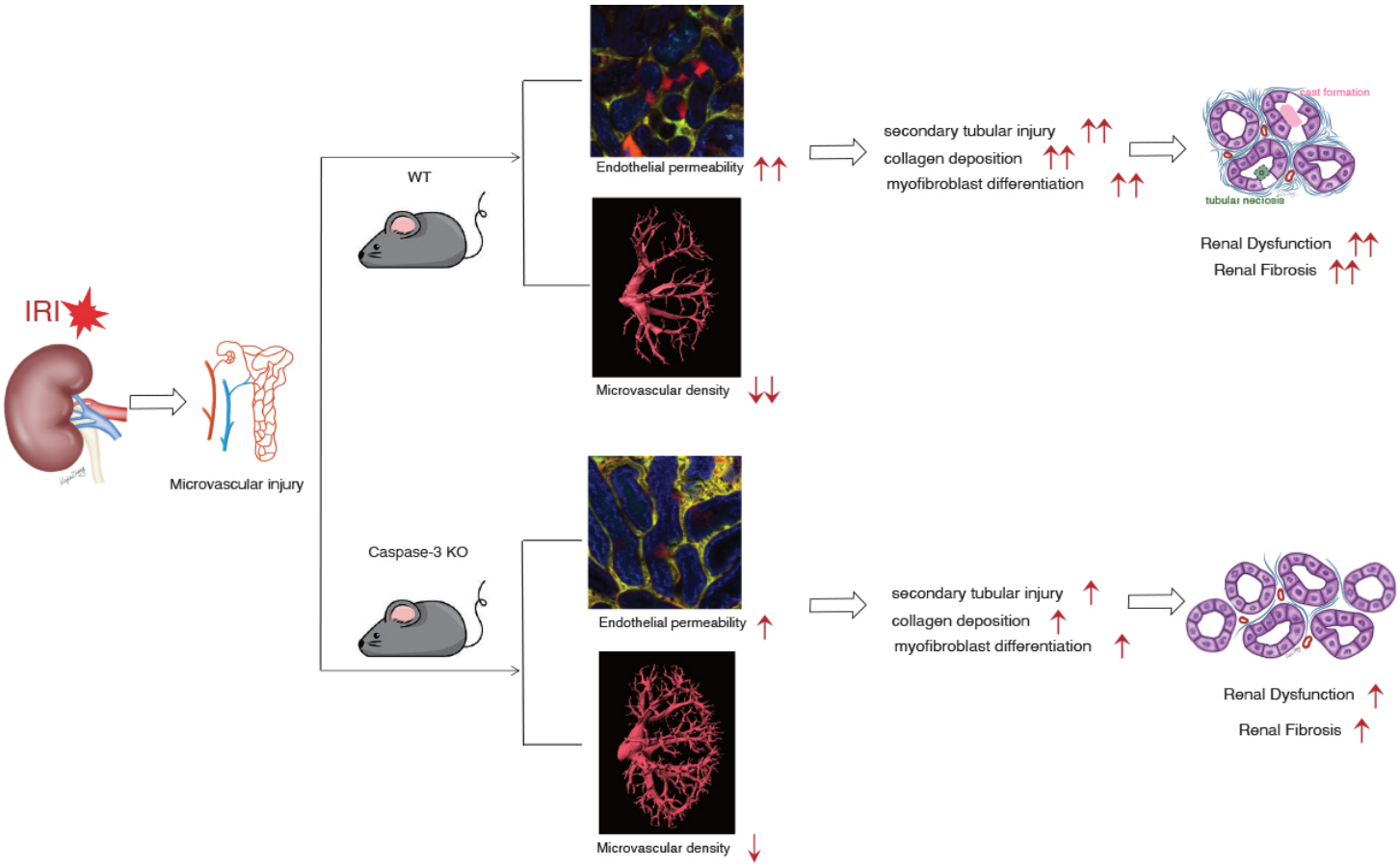

Figure 8: Impact of caspase-3 on microvascular endothelial injury and renal fibrosis and dysfunction post IRI.

Caspase-3 dependent peritubular capillary dysfunction is pivotal for transition from acute to chronic kidney disease after acute ischemia-reperfusion injury

METHODS

Renal ischemia-reperfusion model

WT(C57/Bl6) mice
Caspase-3 general KO mice

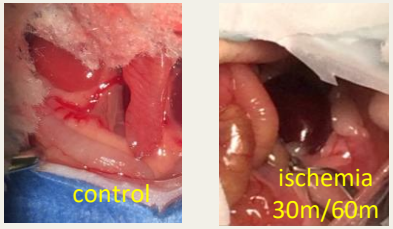

OUTCOME

Caspase-3 deficiency ameliorates renal microvascular dysfunction and fibrosis post ischemia-reperfusion injury (IRI)

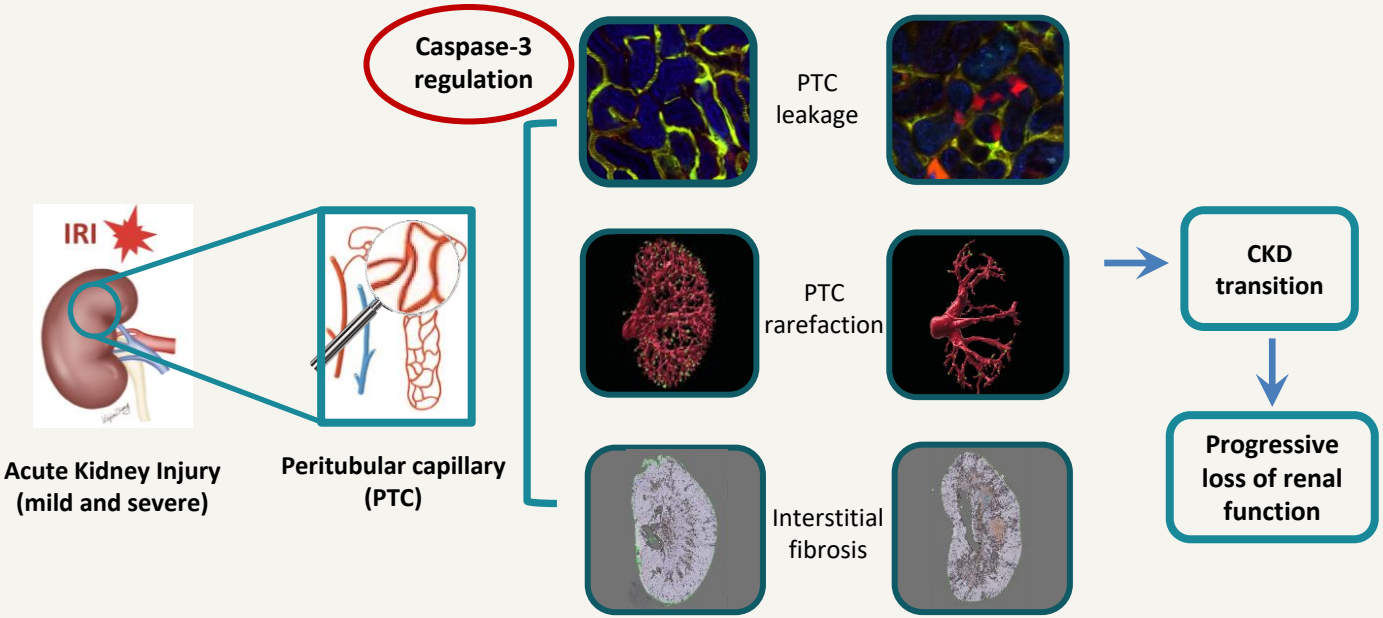

CONCLUSION

The severity of PTC disturbances after ischemia-reperfusion injury is a major predictor of acute kidney injury (AKI) to chronic kidney disease (CKD) transition. Caspase-3 is a central regulator of microvascular rarefaction, fibrogenesis, and long-term renal function.